HHS Public Access

Author manuscript

Glia. Author manuscript; available in PMC 2023 March 01.

Published in final edited form as:

Glia. 2022 March ; 70(3): 451–465. doi:10.1002/glia.24114.

C1q and SRPX2 regulate microglia mediated synapse elimination during early development in the visual thalamus but not the visual cortex

Qifei Cong[1,2,*], **Breeanne M. Soteros**[1], **Anran Huo**[2], **Yang Li**[3], **Andrea J. Tenner**[4,5,6], **Gek Ming Sia**[1,*]

[1]Department of Pharmacology, University of Texas Health Science Center at San Antonio, San Antonio, TX, USA

[2]Institutes of Neuroscience, Soochow University, Suzhou, China.

[3]Department of Neurology, The Second Affiliated Hospital of Soochow University, Suzhou, China.

[4]Department of Molecular Biology and Biochemistry, University of California, Irvine, CA, USA

[5]Department of Neurobiology and Behavior, University of California, Irvine, CA, USA.

[6]Institute for Memory Impairments and Neurological Disorders, University of California, Irvine, CA, USA.

Abstract

The classical complement cascade mediates synapse elimination in the visual thalamus during early brain development. However, whether the primary visual cortex also undergoes complement-mediated synapse elimination during early visual system development remains unknown. Here, we examined microglia-mediated synapse elimination in the visual thalamus and the primary visual cortex of early postnatal C1q and SRPX2 knockout mice. In the lateral geniculate nucleus, deletion of C1q caused a persistent decrease in synapse elimination and microglial synapse engulfment, while deletion of SRPX2 caused a transient increase in the same readouts. In the C1q-SRPX2 double knockout mice, the C1q knockout phenotypes were dominant over the SRPX2 knockout phenotypes, a result which is consistent with SRPX2 being an inhibitor of C1q. We found that genetic deletion of either C1q or SRPX2 did not affect synapse elimination or microglial engulfment of synapses in layer 4 of the primary visual cortex in early brain development. Together, these results show that the classical complement pathway regulates microglia-mediated synapse elimination in the visual thalamus but not the visual cortex during early development of the central nervous system.

Keywords

Complement; Synapse elimination; Microglia engulfment; Visual system

[*]Corresponding author: qfcong@suda.edu.cn, siag@uthscsa.edu.

Declaration of interests

The authors declare no competing interests.

Introduction

During brain development, synapses are constantly formed and eliminated (Grutzendler et al., 2002) via different cell biological processes (Shen and Scheiffele, 2010; Riccomagno and Kolodkin, 2015; Südhof, 2021). Both synapse formation and elimination require communication between neurons and several glial cell types, including astrocytes (Allen and Eroglu, 2017) and microglia (Hammond et al., 2018). This intercellular communication is in turn orchestrated by a variety of molecular mechanisms which vary by brain region and stage of neurodevelopment (Dalva et al., 2007; Riccomagno and Kolodkin, 2015; de Wit and Ghosh, 2016; Wilton et al., 2019). Synapse formation predominates during early development, causing the formation of an excess of synapses, which are eliminated later in development to achieve proper maturation of neural circuitry (Huttenlocher, 1979). While synapse formation and elimination predominate in different stages of development, there is extensive overlap between the two processes in most brain regions. Defects in the extent or timing of either synapse formation or elimination can lead to neurodevelopmental and neurodegenerative disorders (Penzes et al., 2011). Thus, understanding the cellular and molecular mechanisms that regulate synapse formation and elimination can provide insight into the pathogenesis of neuropsychiatric disorders.

Microglial cells are brain-resident macrophages which play an important role in developmental synapse elimination by phagocytosing excess synapses during brain development (Li and Barres, 2018). The molecular mechanisms regulating microglia-mediated synapse elimination during development have recently been intensely investigated. These diverse molecular mechanisms include complement cascade mediated ‘eat me’ signaling (Stevens et al., 2007; Schafer et al., 2012); CD47, SRPX2 mediated “don’t eat me” signaling (Lehrman et al., 2018; Soteros et al., 2018; Cong et al., 2020); chemokine fractalkine CX3CL1-CX3CR1 mediated signaling (Paolicelli et al., 2011; Hoshiko et al., 2012; Gunner et al., 2019); and TREM2 mediated signaling (Filipello et al., 2018). A central molecular mechanism mediating synapse elimination is the complement system (Stevens et al., 2007), which when activated tags weaker synapses for phagocytic clearance via the complement receptor CR3 expressed in microglia (Schafer et al., 2012), a process which has been best demonstrated in the dorsal lateral geniculate nucleus (dLGN) of the visual thalamus. In the visual cortex, during early neurodevelopment, microglial processes have been shown to make dynamic contact with neuronal dendrites, guided by neuronal activity and molecular cues, and engulf and eliminate weaker or immature synapses (Tremblay et al., 2010). However, another study has also shown that in the primary visual cortex, C1q is not required for ocular dominance plasticity in early brain development, and its absence does not affect spine density on most dendrite segments of layer 2/3 pyramidal neurons (Welsh et al., 2020). Thus, despite extensive work on complement and microglia mediated synapse elimination in the developing visual thalamus, it remains unclear whether this pathway acts in the primary visual cortex to mediate synaptic pruning during early brain development.

Here, we investigate the role of the complement-microglia pathway in mediating synapse elimination along the retino-geniculate-cortico visual pathway during early brain development. We alter complement activation in the juvenile mouse brain by genetic deletion of the complement initiating protein C1qa, which decreases complement activation,

or genetic deletion of the neuronal complement inhibitor SRPX2, which increases complement activation. We found that deletion of C1qa leads to a persistent decrease in microglial engulfment of retinal ganglion cell (RGC) afferents and a persistent increase in eye-specific RGC afferent overlap in the dLGN. Conversely, deletion of SRPX2 leads to a transient increase in microglial engulfment of RGC afferents and a transient decrease in eye-specific RGC afferent overlap in the dLGN. In the C1qa-SRPX2 double KO mouse, we found decreased microglial engulfment of RGC afferents and increased eye-specific RGC afferent overlap in the dLGN, consistent with SRPX2 being an inhibitor of C1q. However, knockout of C1qa, SRPX2, or both C1qa and SRPX2 does not affect synapse density or microglial engulfment of synapses in layer 4 of the visual cortex in early development, despite these genetic manipulations showing a clear effect in the visual thalamus. Together, these findings indicate that the complement-microglia pathway drives synapse elimination in the visual thalamus but not the visual cortex during early development.

Materials and Methods

Animal work

All animal work was approved by the University of Texas Health Science Center at San Antonio (UTHSCA) Institutional Animal Care and Use Committee (IACUC).

Mice

Mice were maintained in the UTHSCSA animal facility under a 12 hour light:dark cycle with ad libitum access to food and water. The following lines were used:

SRPX2$^{-/Y}$ mice

The generation of this mouse line has previously been reported (Soteros et al., 2018), and these mice were maintained on a C57BL/6J background. All experiments were performed with male SRPX2$^{-/Y}$ and SRPX2$^{+/Y}$ littermates. As SRPX2 is an X-linked gene, it is not possible to generate female WT and KO pups in the same litter, and random X-inactivation render heterozygous female mice unusable for experiments.

C1qa$^{-/-}$ mice

C1qa$^{tm1c(EUCOMM)Wtsi}$ mice (Jackson 031261) was obtained from Dr. Andrea Tenner's lab (Fonseca et al., 2017). This mouse line contains loxP sites flanking exon 3 of the complement C1qa gene. To generate C1qa knockout mice, C1qa$^{fl/fl}$ mice were crossed with B6N.FVB-Tmem163$^{Tg(ACTB-cre)2Mrt}$/CjDswJ (also known as β-actin-cre mice, Jackson 019099) to generate C1QA knockout alleles in the germline. C1qa knockout mice were backcrossed to C57Bl6/J prior to conducting experiments. For generation of experimental mice, mice were bred as SRPX2$^{-/X}$;C1qa$^{-/+}$ × SRPX2$^{X/Y}$;C1qa$^{-/+}$. All experiments were performed on male littermates.

Labeling of retinogeniculate afferents

Mouse pups (P3 or P9) were anesthetized by hypothermia. Briefly, pups were placed in a glove and immersed in crushed ice and water for 5–7 min. During the surgery, the

hypothermic pups were placed on an ice pack (3–4 ^{O}C). After the surgery, pups were placed in a slide warmer (Thermo Fisher scientific, Waltham, Massachusetts) at 33^{O}C for at least 1 h. Adult mice (P29) were anesthesized with Avertin (0.025 mL/g). Pups and adult mice received intravitreal injections of cholera toxin-β subunit (CTβ) conjugated to Alexa 488 dye (ThermoFisher Scientific, Cat no. C22841, 0.5% in Dulbecco's phosphate buffered saline) into the left eye and cholera toxin-β subunit (CTβ) conjugated to Alexa 555 dye (ThermoFisher Scientific, Cat no. C22843, 0.5% in Dulbecco's phosphate buffered saline) into the right eye. The injection volume for P3 pups was 0.5 μL per eye, while P9 pups and P29 mice received 1 μL per eye. After 24 h, pups and adult mice were dissected for transcardial perfusion with PBS, followed by 4% paraformaldehyde (PFA). Brains were postfixed in 4% PFA for overnight, washed with PBS and rinsed to cryoprotect in 30% sucrose, and then sectioned coronally with a Leica SM2010R sliding microtome at 40 μm, mounted on Superfrost Plus slides (Thermo Fisher Scientific, Waltham, Massachusetts), and coverslipped with Fluoromount-G (SouthernBiotech, Birmingham, AL).

Quantification of lateral geniculate nuclei (LGN) images and preparation of photomicrographs

Images were acquired on a Zeiss AxioObserver microscope with a Zeiss Apotome.2 module, as previously described (Cong et al., 2020). All images were collected and quantified blind, with the same parameters for each label. The five brain sections that contained the largest ipsilateral projections, corresponding to the central dLGN area, were selected for analysis. All analyses were conducted on sections with Alexa 488-labeled contralateral and Alexa 555-labeled ipsilateral projections. Raw images were imported into Image J and cropped to exclude the vLGN and IGL region, then the overlapping area with both contralateral and ipsilateral projections was quantified using the multi-threshold protocol (Torborg and Feller, 2004; Torborg et al., 2005).

RNAscope in situ hybridization (ISH) combined with immunohistochemistry (IHC).

RNAscope ISH on fresh frozen tissue was used to detect SRPX2 mRNA localization. To identify cell type-specific expression, we combined RNAscope mRNA detection with antibody-based IHC. Fresh frozen tissue was used for SPRX2 mRNA with co-staining for neuronal marker NeuN or oligodendrocyte marker Olig2 detection, while paraformaldehyde (PFA)-fixed tissue was used for SRPX2 mRNA with co-staining for microglia marker Iba1 or astrocyte marker GFAP detection. A Leica cryostat was used to cut 20 μm sections of retina and brain, which were mounted on Superfrost Plus slides (ThermoFisher Scientific, 4951PLUS-001). RNAscope ISH was performed on both tissue preparations according to the manufacturer instructions (ACDBio RNAscope® 2.5 HD Reagent Kit-RED, Cat. no. 322350) with slight modifications. Briefly, tissues were pretreated separately with hydrogen peroxide for 10 min and Protease Plus for 30 min at RT followed by a wash in PBS. SRPX2 probe (RNAscope® probe Mm-SRPX2, Cat. no. 802711) was incubated with tissues at 40 °C for 2 h. Subsequent amplification steps were performed according to the manufacturer instructions. After the chromogen development step, the slides were washed with PBS and PBST (1x PBS containing 0.25% Triton X-100) once separately, and further blocked with PBST containing 2% normal goat serum for 1 h at RT. Primary antibodies of cell-specific marker NeuN (EMD Millipore, Cat. no. ABN91, 1:500), Iba1 (Wako Chemicals,

Cat. no. 019-19741, 1:500), GFAP (EMD Millipore, Cat. no. AB5541, 1:500) and Olig2 (Abcam, Cat. no. ab109186, 1:500) and subsequent incubation with secondary antibodies and DAPI were both prepared in PBST containing 2% normal goat serum. Primary antibody incubations were performed for overnight at 4 °C, and secondary antibody incubations were performed for 1 hr at room temperature. Secondary antibodies include goat anti-mouse IgG1 Alexa 488 (Thermo Fisher, A-21121), donkey anti-chicken IgY Alexa 488 (Jackson ImmunoResearch, 703-545-155), goat anti-rabbit Alexa 488 (Thermo Fisher, A-11034), and DAPI (ThermoFisher Scientific, Cat. no. D1306). After final washes with PBST and PBS, slides were cover-slipped with Fluoromount-G (Southern Biotech). Images were acquired with a Zeiss Observer Z1 inverted microscope (Zeiss Objective Plan-Apochromat 63x/1.4 Oil) with a Zeiss Apotome.2 module. All images were acquired in 63x magnification and analyzed using Image J (NIH).

Immunohistochemistry.

The following IHC protocol was performed to stain for SRPX2, NeuN, complement protein, synapse density, and microglial engulfment of synapses. Mice were anesthetized with Avertin (0.5 mg/g) and transcardially perfused with ice-cold PBS and 4% paraformaldehyde (PFA). Brains and eyes were dissected and immediately post-fixed in 4% PFA for overnight at 4°C, then cryoprotected in 30% sucrose in PBS for 2–3 days, and then sectioned at 40 μm. Free-floating sections were first washed with 0.2% TX-100 in PBS (PBT) then blocked 1 hr at RT in 10% normal donkey/goat serum (Jackson Immunoresearch) in PBT. Slices were reacted with primary antibodies overnight at 4°C, washed with PBT for 3 times, then incubated with secondary antibodies and DAPI for 2 hr at room temperature. Sections were further washed 3x in PBT and 3x in PBS. The slices were free-floated onto Superfrost Plus glass slides and cover-slipped with Fluoromount-G (Southern Biotech). The following primary antibodies were used: mouse IgG2b anti-SRPX2 (Creative Biolabs, CBMAB-S1587-CQ, 1:1500), rabbit anti-NeuN (Proteintech, 26975-1-AP, 1:1000), rabbit anti-C1q (Abcam, ab182451 1:1000), goat anti-rat C3 (MP Bio, 0855730 1:1000), guinea pig anti-VGlut1 (Synaptic Systems, 135–304, 1:2500), guinea pig anti-VGlut2 (Synaptic Systems, 135–404, 1:2500), mouse IgG1 anti-PSD95 (Synaptic Systems, 124–011, 1:500), guinea pig anti-VGat (Synaptic Systems, 131–004, 1:500), mouse IgG1 anti-gephyrin (Synaptic Systems, 147–021,1:500), rabbit anti-Iba1 (Wako Chemicals, 019–19741 1:1000), rat anti-CD68 (Bio-Rad, MCA1957, 1:1000). Secondary antibodies include: goat anti-rabbit Alexa 488 (Thermo Fisher, A-11034), donkey anti-rat Alexa 647 (Jackson ImmunoResearch 712-605-153), goat anti-guinea pig Alexa 555 (Thermo Fisher Scientific, A-21435), goat anti-mouse IgG2b Alexa 555 (Fisher scientific, Cat. no. A21147), goat anti-mouse IgG2a Alexa 488 (Fisher scientific, Cat. no. A21131), Cy5 AffiniPure donkey anti-guinea pig (Jackson, 706-105-148), Cy5 AffiniPure donkey anti-goat (Jackson, Cat. no. 705-175-147), goat anti-mouse IgG1 Alexa 488 (Thermo Fisher, A-21121), and DAPI (ThermoFisher Scientific, Cat. no. D1306). All secondary antibodies and DAPI were used at a concentration of 1:500.

Colocalization, complement deposition & synapse density analysis.

Images were acquired with a Zeiss AxioObserver inverted microscope (Zeiss Objective Plan-Apochromat 63x/1.4 Oil) equipped with a Zeiss Apotome.2 module and Zeiss Plan-

Apochromat 63x/1.4 oil objective. Identical imaging parameters were used for all genotypes for the comparative analysis. To measure C1q and C3 deposits, and determine synapse density, ImageJ (NIH) was used for image processing. Individual channels were first Z-projected with summation over a depth of 3 μm and background-subtracted. Threshold channels were empirically determined and then consistently applied to each channel for all subjects. For quantifying C1q and C3 deposits, the Analyze Particles tool was used to quantify the number of individual C1q & C3 puncta. For synapse density, colocalized puncta were first obtained by using the image calculator tool to multiply the individual pre & post-synaptic channels, and the resulting image was then quantified with the Analyze Particles tool.

Microglial engulfment assays.

CTB engulfment in the dLGN and VGlut2 engulfment in layer 4 of the primary visual cortex as previously described (Cong et al., 2020). Three dimensional reconstructions of microglia were derived from high resolution confocal images of Iba1 cells using the Imaris software (version 9.2, Bitplane, Concord MA). Using the image processing tool in Imaris, background subtraction was performed on all channels, followed by a Gaussian filter. Iba1-positive cells were surface rendered with 0.1 μm smoothing. Disconnected processes were merged with the cell body to create a single surface. A mask was applied to the surface rendered microglia for the channel containing CD68 to isolate the CD68 signal only within the microglia for surface rendering (0.1 μm smoothing). For CTB and VGlut2 engulfment assays, a mask was applied to the surface rendered CD68 within microglia for either the CTB or VGlut2 channels to reveal only the CTB or VGlut2 signal within microglial lysosomes. The isolated CTB or VGlut2 channels were surfaced rendered with 0.1 μm smoothing. The volume of the reconstructed surfaces for Iba1, CD68, CTB or VGlut2 were recorded. The % engulfment of CTB or VGlut2 within microglial lysosomes was calculated using the formula: volume of engulfed material found in lysosome/volume of $Iba1^{+}$ cell.

Statistics

GraphPad Prism v8 was used for all statistical analyses. All measurements were taken from blinded samples. No data points were excluded from analysis. When comparing two conditions, unpaired two-tailed Student’s t-test were used. When comparing more than two conditions, one-way ANOVA was performed, followed by two-tailed Dunnett’s post-hoc test comparing all means to the control $SRPX2^{+/Y}$ mean. Data of $SRPX2^{+/Y}$ and $SRPX2^{-/Y}$ used in eye specific segregation analysis are the same batch analyzed in previous study (Cong et al., 2020). Eye specific segregation curves were analyzed with two-way ANOVA, with two-tailed Dunnett’s post-hoc test. All images shown in figures are representative images of data quantified in the corresponding graphs.

Results

C1q is required for the effect of SRPX2 on retinogeniculate refinement

Refinement of retinogeniculate axons in the dorsal lateral geniculate nucleus (dLGN) of the visual thalamus is a classic model system for the study of developmental synapse elimination. It has previously been shown that genetic deletion of the complement initiator

C1qa causes a decrease in the refinement of retinogeniculate synapses in the dLGN (Stevens et al., 2007), and the deletion of the complement inhibitor SRPX2 causes an increase in retinogeniculate synapse refinement (Cong et al., 2020). While it has been shown that SRPX2 binds to C1q and inhibits the activation of C1r and C1s proteolytic activity *in vitro*, it is unclear *in vivo* whether SRPX2 acts through C1q to exert its effect on synapse elimination. To test whether the effect of SRPX2 on synapse refinement is dependent on C1q activity, we generated mice of four genotypes: wildtype, SRPX2$^{-/Y}$ knockout, C1qa$^{-/-}$ knockout, and C1qa$^{-/-}$;SRPX2$^{-/Y}$ double knockout mice. To assess retinogeniculate axon refinement in the dLGN, we injected cholera toxin B (CTB) conjugated to Alexa 488 or Alexa 555 dyes into the left or right eyes of mice respectively at P3, P9 and P29. After 24 hours, we fixed and sectioned the brains for imaging (Figure 1A, C and E). To quantitate the synapse refinement in the developing dLGN for the four mouse lines, we measured the overlapping area between contralateral and ipsilateral axon projections. In wildtype mice, axons from the ipsilateral and contralateral eyes largely overlap at P4 (Figure 1A, B), begin to segregate at P10 (Figure 1C, D), and almost completely segregate into eye-specific domains by P30 (Figure 1E, F), a time point at which the eye-specific domains are similar to that in adulthood (Huberman et al., 2008; Assali et al., 2014). In SRPX2$^{-/Y}$ knockout mice, contralateral and ipsilateral retinogeniculate inputs in the dLGN are already partially segregated at P4 (Figure 1A, B), a time point before eye-specific segregation occurs in wildtype mice. By P10, axon segregation has reached near-maximal levels in the SRPX2 (Figure 1C, D). However, by P30, axon segregation in wildtype mice has caught up to that in SRPX2$^{-/Y}$ knockout mice, suggesting that presence of a ceiling effect in this assay. In C1qa$^{-/-}$ knockout mice, axon refinement is impaired compared to wildtype mice starting at P10 (Figure 1C, D), and this impairment persists to P30 (Figure 1E, F). The C1qa$^{-/-}$;SRPX2$^{-/Y}$ double knockout mice showed a similar phenotype to C1qa$^{-/-}$ knockout mice at every time point assessed (Figure 1B, D, F), indicating that C1q is required for the effect of SRPX2 deletion on LGN synapse elimination. Thus, we replicated previous reports that C1qa deletion decreases axon segregation (Stevens et al., 2007) while SRPX2 deletion increases axon segregation (Cong et al., 2020) in the dLGN. We further showed that in SRPX2$^{-/Y}$ knockout mice, C1qa co-deletion reversed SRPX2's effect on axon refinement in the dLGN at all time points. These results are consistent with SRPX2 being an inhibitor of C1q, and in the absence of C1q, SRPX2 no longer exerts an effect on synapse elimination.

Effect of SRPX2 on microglial engulfment is dependent on C1q in the dLGN

Complement proteins act as 'eat me' signals in the brain, directing microglia to engulf immature synapses during development (Schafer et al., 2012). Our previous study showed that SRPX2 deletion increased microglial engulfment of synapse in the dLGN in a C3-dependent manner (Cong et al., 2020). However, it remains unclear if the effect of SRPX2 on microglial engulfment is dependent on C1q. To assess microglial engulfment of synapses in the dLGN, we injected Alexa 555 conjugated CTB into both eyes of mice intravitreously at P3, P9 and P29. After 24 hours, we fixed and sectioned the brains, and stained the brain sections for microglial marker Iba1 and lysosome marker CD68 (Figure 2A, Supplementary Figure 1). Individual microglia cells within the core region of the dLGN were randomly selected and imaged at high resolution, and a 3D reconstruction of the microglia was created. The volume of CTB tracer contained within CD68 positive and Iba1

positive microglial lysosomes was quantitated. In this assay, SRPX2$^{-/Y}$ mice show increased levels of microglial retinogeniculate synapse engulfment at P4 and P10, which declines to wildtype levels by P30 (Figure 2B–D). C1qa$^{-/-}$ mice had persistently decreased levels of microglial retinogeniculate synapse engulfment at all three time points (Figure 2B–D). C1qa$^{-/-}$;SRPX2$^{-/Y}$ mice showed reduced levels of microglial axon engulfment similar to the C1qa$^{-/-}$ mice at all time points (Figure 2B–D). Thus, these results show that SRPX2's effect on microglial engulfment of synapses in the dLGN requires the presence of C1q.

Expression pattern of SRPX2 in the developing visual retino-geniculo-cortical pathway

In the visual system, light information received by the retina is transmitted by retinal ganglion cells (RGCs) to relay neurons in the LGN, which in turn transmit visual information to the primary visual cortex. After assessing the effect of C1q and SRPX2 deletion on synapse elimination and microglial engulfment in the LGN, we wanted to examine if these processes are also altered in the primary visual cortex. As development of circuitry in the primary visual cortex can potentially be affected by changes in other brain regions caused by deletion of complement genes, we set out to characterize the expression of complement-related genes in the retino-geniculo-cortical pathway. As it has already previously been shown that C1q is present in the entire retino-geniculo-cortical pathway (Stevens et al., 2007; Bialas and Stevens, 2013; Welsh et al., 2020), we focused on examining the expression of SRPX2 in the retina, dLGN, and primary visual cortex, using RNAscope fluorescent in situ hybridization (ISH) to detect SRPX2 mRNA, combined with DAPI counterstaining to show nuclei. We found that at P4, SRPX2 mRNA is distributed over multiple layers of the retina, including in the ganglion cell layer (Figure 3A). As development progresses, SRPX2 mRNA gradually becomes localized to the inner nuclear layer at P10 and P30 (Figure 3A). As the dLGN RGC axon refinement phenotype of SRPX2$^{-/Y}$ knockout mice is maximal at P4, we combined RNAscope ISH with immunostaining for cell-specific markers in order to determine if SRPX2 mRNA is localized to RGCs in the ganglion cell layer at P4. We found that SRPX2 mRNA in the ganglion cell layer at P4 are mainly colocalized with cell bodies that are positive for the neuronal marker NeuN, with a small percentage of SRPX2 mRNA also colocalized with the astrocyte marker GFAP, but no SRPX2 mRNA are found in cell bodies that are positive for the microglia marker Iba1 or the oligodendrocyte marker Olig2 (Figure 3B, C). These results show that at P4, SRPX2 is primarily expressed in retinal ganglion cells.

To determine if SRPX2 is also expressed primarily in neurons in the dLGN and primary visual cortex, we also performed RNAscope ISH in these brain regions, combined with IHC for the neuronal marker NeuN. In both the dLGN and the primary visual cortex, we observed that SRPX2 mRNA is localized primarily to NeuN-positive neuronal soma (Figure 3C). These results show that SRPX2 is expressed primarily in neurons throughout the retino-geniculo-cortical pathway.

To verify that SRPX2 is expressed in neurons, we also performed immunostaining for SRPX2 protein and the neuronal marker NeuN in the P4 retina (Figure 3E), dLGN (Figure 3F), and visual cortex (Figure 3G). The results show that SRPX2 protein is present in NeuN positive neurons in all 3 brain regions.

C1q and SRPX2 do not regulate synapse elimination in layer 4 of the visual cortex in early development

The primary visual cortex receives input from relay cells in the dLGN, which sends axons that terminate mainly in layer 4 of the visual cortex. To further characterize the contribution of C1q to synapse elimination in layer 4 of the primary visual cortex during early development, we assessed synapse density in that region in wildtype, SRPX2$^{-/Y}$ knockout, C1qa$^{-/-}$ knockout, and C1qa$^{-/-}$;SRPX2$^{-/Y}$ double knockout mice, at P4, P10 and P30. We assessed synapse density in layer 4 of the primary visual cortex by staining for the corticocortical synapse markers VGlut1/PSD95, the thalamocortical synapse markers VGlut2/PSD95, and the inhibitory synapse markers VGAT/gephyrin. To our surprise, despite the clear phenotypes in synapse elimination in the dLGN, layer 4 synapse densities for all markers assessed were comparable to wildtype levels at all time points for all genotypes (Figure 4A–F). This suggests that synapse elimination in the layer 4 of the primary visual cortex proceeds normally despite the molecular perturbations in the knockout mice, and despite the circuitry changes in the LGN region. These results indicate that the major types of synapses in layer 4 of the primary visual cortex develop normally even after genetic deletion of C1qa or SRPX2 deletion, and that the classical complement pathway is not required for synapse elimination in visual cortex during early development.

SRPX2 deletion does not alter complement activation in layer 4 of the visual cortex in early development

We have previously found that deletion of SRPX2 in the developing dLGN leads to a transient increase in complement activation, resulting in excessive complement-mediated microglial engulfment of synapses. To understand whether loss of SRPX2 also leads to complement activation in the visual cortex, we performed IHC for C1q and C3 on brain slices from SRPX2$^{+/Y}$ and SRPX2$^{-/Y}$ mice at P4, P10, and P30 (Figure 5A, C), and quantitated the levels of C1q and C3 in layer 4 of the primary visual cortex (Figure 5B, D). We found that SRPX2$^{-/Y}$ mice has levels of C1q and C3 in layer 4 that are comparable to levels in wildtype SRPX2$^{+/Y}$ mice at all time points (Figure 5B, D). These data indicate that complement activity levels in the early developing visual cortex are not sensitive to SRPX2 expression. We speculate that SRPX2 deletion does not lead to excess complement activation in the primary visual cortex because layer 4 synapses are not actively undergoing complement-mediated synapse elimination at this early developmental time point.

C1q and SRPX2 do not regulate microglial engulfment of synapses in the layer 4 of the visual cortex during early development

Previous studies indicate that microglial engulfment of synapses occurs in the primary visual cortex during early development on or before P30 (Tremblay et al., 2010; Ding et al., 2021). While genetic deletion of C1qa and SRPX2 did not cause a detectable change in synapse density, microglial engulfment of synapses may be a more sensitive readout. Given that VGlut2 positive thalamocortical synapses has been found to be engulfed by microglia in other cortical regions (Soteros et al., 2018; Cong et al., 2020; Yilmaz et al., 2021), we assessed microglial engulfment of VGlut2 synapses in layer 4 of the primary visual cortex. We performed IHC for the thalamocortical synapse marker VGlut2, microglial marker Iba1,

and lysosome marker CD68 on brain slices from wildtype, SRPX2$^{-/Y}$ knockout, C1qa$^{-/-}$ knockout, and C1qa$^{-/-}$;SRPX2$^{-/Y}$ double knockout mice, at P4, P10 and P30. Image stacks of individual microglia in layer 4 of the visual cortex were 3D-rendered, and the amount of VGlut2 within Iba1 and CD68-positive microglial lysosomes was quantified. For all 4 genotypes assessed, at all time points, microglial engulfment of synapses is nearly identical (Figure 6, Supplementary Figure 2). These results indicate that the classical complement pathway does not regulate microglial engulfment of synapses in the visual cortex during early development.

Discussion

Synapse formation and elimination occurs continuously in the brain, and these processes are especially dynamic during early development. Complement- and microglia-dependent synapse elimination has been shown to play an important role in the development of the visual thalamus (Stevens et al., 2007; Schafer et al., 2012). However, whether the complement pathway plays a role in synapse elimination in the developing cortex remains unclear. Here, we show that during early development before P30, genetic deletion of C1qa or SRPX2 affects synapse elimination and microglial engulfment of synapses in the dLGN but not the visual cortex. We also show that the effect of SRPX2 on thalamic synapse elimination requires the presence of C1q, consistent with its role as an inhibitor of C1 protease activity (Cong et al., 2020). Our results suggest that the regulation of developmental synapse elimination by the classical complement pathway varies depending on the brain region and time point, and that in the early developing visual system, the classical complement pathway regulates synapse elimination in the visual thalamus but not the visual cortex.

Complement-dependent signaling in synapse elimination

Synapse elimination occurs continuously throughout brain development, but at different rates during different development periods. Many brain regions go through a maturation process comprising of 2 developmental periods, an initial period of net synapse formation when the rate of synapse formation exceeds that of synapse elimination, followed by a period of net synapse elimination when the rate of synapse elimination exceeds that of synapse formation (Huttenlocher, 1979; Rakic et al., 1986). An outstanding question in developmental neuroscience is whether similar molecular and cellular mechanisms subserve synapse elimination in both developmental periods, or whether the brain engages different mechanisms in different periods. In the visual thalamus, both developmental periods are completed by P30 (Huberman et al., 2008), and extensive research has shown that the complement-microglia pathway mediates synapse elimination from P10 to P30 in the visual thalamus, coincident with the period of net synapse elimination (Stevens et al., 2007; Schafer et al., 2012; Bialas and Stevens, 2013; Sekar et al., 2016; Cong et al., 2020). In the mammalian cortex, the period of net synapse elimination occurs in adolescence (Huttenlocher, 1979; Rakic et al., 1986; Pinto et al., 2013), which occurs after P30 in rodents. A pair of early studies on C1qa knockout mice on the P30 sensorimotor cortex found that layer 5 pyramidal neurons in these mice had increased dendritic spine densities and greater responses to uncaged glutamate in layer 4 and 5 (Chu et al., 2010; Ma et al.,

2013), suggesting that there is a defect in developmental synapse pruning in the cortex of C1qa knockout mice. We had also found that in the P60 to P90 somatosensory cortex, layer 4 thalamocortical synapses are eliminated via the complement-microglial pathway (Cong et al., 2020). Complement-dependent synapse elimination has also been observed outside of the developmental time periods, in both the adult animal, as well as in pathological situations. In the adult hippocampus, complement-dependent synapse elimination has been implicated in mediating the forgetting of memories (Wang et al., 2020), and complement-dependent elimination of hippocampal synapses has been implicated in virus induced amnesia (Vasek et al., 2016) and Alzheimer's disease associated memory loss (Hong et al., 2016; Shi et al., 2017). In the thalamus, complement-dependent synapse losses in the ventral and visual thalamus have also been observed in mouse models of frontal temporal dementia (FTD) and multiple sclerosis (MS) respectively (Lui et al., 2016; Werneburg et al., 2020). In the cortex, excessive synapse elimination in the human juvenile cortex has also been implicated in the pathogenesis of schizophrenia (Sekar et al., 2016; Sellgren et al., 2017; Yilmaz et al., 2021). Thus, current evidence suggest that complement-microglial synapse elimination is a major mechanism for synapse removal in multiple brain regions during the developmental period of net synapse elimination, as well as in adulthood and in many pathological situations.

Mechanisms of synapse elimination during early development

While the rate of synapse elimination peaks during the developmental period of net synapse elimination, synapse elimination occurs in the cortex even during the earlier period of net synapse formation. Indeed, microglial phagocytosis of synapses has been observed in the visual cortex in P28-P32 mice, and light deprivation caused microglia to become less motile and more associated with larger dendritic spines (Tremblay et al., 2010). However, there have been conflicting reports on whether early synapse elimination in the cortex is also dependent on complement. Increased spine densities have been reported layer 5 neurons in the P30 sensorimotor cortex of C1qa knockout mice (Chu et al., 2010; Ma et al., 2013), but in the primary visual cortex of the same mice, spine densities of layer 2/3 neurons were largely unchanged, and ocular dominance plasticity in the visual cortex is also intact (Welsh et al., 2020), suggesting that C1q does not regulate synapse elimination in the P30 visual cortex but does so in the sensorimotor cortex. Another study found that whisker trimming in the P4 to P10 mouse causes synapse loss and microglial phagocytosis of synapses in the somatosensory cortex, which are blocked by CX3CR1 deletion but not CR3 deletion, indicating that the synapse elimination in this system is complement-independent and is instead dependent on the fractalkine signaling pathway (Gunner et al., 2019). In this study, we found that genetic deletion of C1qa or SRPX2 does not affect synapse density or microglial synapse engulfment in layer 4 of the primary visual cortex, despite the same genetic perturbations showing clear effects on synapse elimination in the dLGN. While differences in experimental paradigms, brain regions, or time points may account for the discrepancies among studies, our results suggest that during the initial period of net synapse formation, microglial phagocytosis of synapses occurs but is not mediated by complement signaling.

Other molecular mechanisms regulating microglial phagocytosis of synapses

In addition to the complement system, multiple other molecular mechanisms are also known to regulate microglial phagocytosis of synapses. These mechanisms include CX3CL1-CX3CR1 fractalkine signaling (Paolicelli et al., 2011; Zhan et al., 2014; Gunner et al., 2019), SIRPα-CD47 signaling (Lehrman et al., 2018; Ding et al., 2021), IL-33 (Vainchtein et al., 2018), TREM2 (Filipello et al., 2018), GPR56 (Li et al., 2020), and MERTK (Park et al., 2021). The CX3CL1-CX3CR1 fractalkine signaling pathway is believed to recruit microglia to neurons in the developing brain, and mice lacking the fractalkine receptor CX3CR1 show a transient increase in hippocampal CA1 pyramidal dendritic spine density at P15 which normalizes by P40 (Paolicelli et al., 2011). Furthermore, in the P4 to P10 somatosensory cortex, activity deprivation by whisker trimming causes synapse elimination of VGlut2 synapses in the deprived somatosensory cortex and increased microglial phagocytosis of VGlut2 synapses, which are blocked by genetic deletion of CX3CR1, but not by deletion of the complement receptor CR3 (Gunner et al., 2019). These results suggest that the fractalkine signaling pathway may be a key regulator of microglial synapse phagocytosis during early postnatal development of the cortex. However, an ultrastructural and live imaging study of the visual cortex in CX3CR1 knockout mice at P15 to P60 reported that genetic deletion of CX3CR1 does not affect microglial motility or contact with dendritic spines at these ages (Lowery et al., 2017), and ocular dominance plasticity in the visual cortex induced by eyelid suturing in the P28 juvenile mouse is similarly unaffected in the CX3CR1 knockout mouse (Lowery et al., 2017; Schecter et al., 2017). While these studies utilize mouse models and readouts which are associated with synapse elimination, they do not directly measure developmental synapse elimination in the visual cortex, and more work is required to probe the role of the fractalkine signaling pathway in the early development of the visual cortex. Another possible molecular mechanism is the SIRPα-CD47 “don’t eat me” signaling pathway, which has been shown to protect synapses in the dLGN from microglial phagocytosis during development (Lehrman et al., 2018). In the microglia-specific SIRPα knockout mouse and the CD47 conventional knockout mouse, VGlut1 synapse density in the visual cortex is normal at P5 and P15 but is decreased at P30 (Ding et al., 2021), suggesting that the SIRPα-CD47 may be a key regulator of synapse elimination in the visual cortex before P30. Finally, astrocytes have also been found to engulf synapses in early development, through the MEGF10/MERTK pathway (Chung et al., 2013). Indeed, astrocytic engulfment of retinogeniculate afferents in the P5-P9 LGN greatly exceeds microglial engulfment of the same afferents due largely to the greater abundance of astrocytes (Chung et al., 2013), suggesting that astrocytic removal of synapses may be a major mechanism in synapse elimination in early development.

The complement system in retinal disease

Mounting evidence implicates complement activation and synapse loss in the pathogenesis of degenerative retinal diseases such as glaucoma and age-related macular degeneration (AMD) (Rosen and Stevens, 2010; Kawa et al., 2014). Glaucoma is characterized by degeneration of retinal ganglion cells associated with elevated intraocular pressure, but is also accompanied by alterations of neural circuits in higher visual areas such as the LGN and visual cortex (Rosen and Stevens, 2010). Complement C1q is upregulated in the retina of glaucomatous DBA/2J mice (Stevens et al., 2007), as well as in the retinas of monkeys

and humans with glaucoma (Stasi et al., 2006). Genetic or pharmacological inhibition of complement C1q (Williams et al., 2016), C5 (Reinehr et al., 2019) and C3aR1 (Harder et al., 2020) are sufficient to reduce axon degeneration and RGCs loss in glaucoma mouse models. AMD is a leading cause of vision loss in the aged population in developed countries, and polymorphisms in complement factor H has been strongly associated with AMD risk (Edwards et al., 2005; Haines et al., 2005; Klein et al., 2005). Despite promising genetic and preclinical data, the use of complement-directed drugs for clinical treatment of retinal diseases has been complicated by the complex effects of the complement pathway in the brain. While complement activation is associated with synapse and neuronal loss, under some conditions, both C1q (Benoit and Tenner, 2011; Schartz and Tenner, 2020) and C3 (Harder et al., 2017) can also be neuroprotective. Gaining a comprehensive understanding of the effect of C1q and its regulators on the development of the visual system will be helpful in understanding its role in diseases of the visual system, and may aid the development of anti-complement therapeutics in these diseases.

Supplementary Material

Refer to Web version on PubMed Central for supplementary material.

Acknowledgements

We thank Matthew Baum (Beth Stevens's lab, Harvard) for technical advice on eye injections. CRISPR/Cas9 pronuclear injections were performed at the Johns Hopkins Transgenic Core Laboratory, and screening of founders and subsequent work was performed at UTHSCSA. This work was supported by NINDS-R01NS112389, the William and Ella Owens Medical Research Foundation, the NARSAD Young Investigator grant number 25248, the UTHSCSA Dept. of Pharmacology, and the Rising STARs award from the University of Texas System to GMS, NIA-R01AG060148 to AJT, and startup funding NH21500221 to QC. Images were generated at the Core Optical Imaging Facility which is supported by UTHSCSA, NCI-P30CA54174 (CTRC at UTHSCSA) and NIA-P01AG19316.

References

Allen NJ, Eroglu C. 2017. Cell Biology of Astrocyte-Synapse Interactions. Neuron 96:697–708. [PubMed: 29096081]

Assali A, Gaspar P, Rebsam A. 2014. Activity dependent mechanisms of visual map formation--from retinal waves to molecular regulators. Semin Cell Dev Biol 35:136s awa

Benoit ME, Tenner AJ. 2011. Complement protein C1q-mediated neuroprotection is correlated with regulation of neuronal gene and miRNA expression. J Neurosci 31:3459–3469. [PubMed: 21368058]

Bialas AR, Stevens B. 2013. TGF-lement protein C1q-mediated neuroprotection is correlated with regulation of neuronal gene and miRNA expression

Chu Y, Jin X, Parada I, Pesic A, Stevens B, Barres B, Prince DA. 2010. Enhanced synaptic connectivity and epilepsy in C1q knockout mice. PNAS 107:7975–7980. [PubMed: 20375278]

Chung W-S, Clarke LE, Wang GX, Stafford BK, Sher A, Chakraborty C, Joung J, Foo LC, Thompson A, Chen C, Smith SJ, Barres BA. 2013. Astrocytes mediate synapse elimination through MEGF10 and MERTK pathways. Nature 504:394–400. [PubMed: 24270812]

Cong Q, Soteros BM, Wollet M, Kim JH, Sia G-M. 2020. The endogenous neuronal complement inhibitor SRPX2 protects against complement-mediated synapse elimination during development. Nat Neurosci 23:1067–1078. [PubMed: 32661396]

Dalva MB, McClelland AC, Kayser MS. 2007. Cell adhesion molecules: signalling functions at the synapse. Nat Rev Neurosci 8:206emen [PubMed: 17299456]

Ding X, Wang J, Huang M, Chen Z, Liu J, Zhang Q, Zhang C, Xiang Y, Zen K, Li L. 2021. Loss of microglial SIRPα promotes synaptic pruning in preclinical models of neurodegeneration. Nat Commun 12:2030. [PubMed: 33795678]

Edwards AO, Ritter R, Abel KJ, Manning A, Panhuysen C, Farrer LA. 2005. Complement factor H polymorphism and age-related macular degeneration. Science 308:421–424. [PubMed: 15761121]

Filipello F, Morini R, Corradini I, Zerbi V, Canzi A, Michalski B, Erreni M, Markicevic M, Starvaggi-Cucuzza C, Otero K, Piccio L, Cignarella F, Perrucci F, Tamborini M, Genua M, Rajendran L, Menna E, Vetrano S, Fahnestock M, Paolicelli RC, Matteoli M. 2018. The Microglial Innate Immune Receptor TREM2 Is Required for Synapse Elimination and Normal Brain Connectivity. Immunity 48:979–991.e8. [PubMed: 29752066]

Fonseca MI, Chu S-H, Hernandez MX, Fang MJ, Modarresi L, Selvan P, MacGregor GR, Tenner AJ. 2017. Cell-specific deletion of C1qa identifies microglia as the dominant source of C1q in mouse brain. J Neuroinflammation 14:48. [PubMed: 28264694]

Grutzendler J, Kasthuri N, Gan W-B. 2002. Long-term dendritic spine stability in the adult cortex. Nature 420:812–816. [PubMed: 12490949]

Gunner G, Cheadle L, Johnson KM, Ayata P, Badimon A, Mondo E, Nagy MA, Liu L, Bemiller SM, Kim K-W, Lira SA, Lamb BT, Tapper AR, Ransohoff RM, Greenberg ME, Schaefer A, Schafer DP. 2019. Sensory lesioning induces microglial synapse elimination via ADAM10 and fractalkine signaling. Nat Neurosci 22:1075–1088. [PubMed: 31209379]

Haines JL, Hauser MA, Schmidt S, Scott WK, Olson LM, Gallins P, Spencer KL, Kwan SY, Noureddine M, Gilbert JR, Schnetz-Boutaud N, Agarwal A, Postel EA, Pericak-Vance MA. 2005. Complement factor H variant increases the risk of age-related macular degeneration. Science 308:419–421. [PubMed: 15761120]

Hammond TR, Robinton D, Stevens B. 2018. Microglia and the Brain: Complementary Partners in Development and Disease. Annu Rev Cell Dev Biol 34:523l EA, [PubMed: 30089221]

Harder JM, Braine CE, Williams PA, Zhu X, MacNicoll KH, Sousa GL, Buchanan RA, Smith RS, Libby RT, Howell GR, John SWM. 2017. Early immune responses are independent of RGC dysfunction in glaucoma with complement component C3 being protective. Proc Natl Acad Sci U S A 114:E3839–E3848. [PubMed: 28446616]

Harder JM, Williams PA, Braine CE, Yang HS, Thomas JM, Foxworth NE, John SWM, Howell GR. 2020. Complement peptide C3a receptor 1 promotes optic nerve degeneration in DBA/2J mice. J Neuroinflammation 17:336. [PubMed: 33176797]

Hong S, Beja-Glasser VF, Nfonoyim BM, Frouin A, Li S, Ramakrishnan S, Merry KM, Shi Q, Rosenthal A, Barres BA, Lemere CA, Selkoe DJ, Stevens B. 2016. Complement and microglia mediate early synapse loss in Alzheimer mouse models. Science 352:712–716. [PubMed: 27033548]

Hoshiko M, Arnoux I, Avignone E, Yamamoto N, Audinat E. 2012. Deficiency of the microglial receptor CX3CR1 impairs postnatal functional development of thalamocortical synapses in the barrel cortex. J Neurosci 32:15106–15111. [PubMed: 23100431]

Huberman AD, Feller MB, Chapman B. 2008. Mechanisms Underlying Development of Visual Maps and Receptive Fields. Annual Review of Neuroscience 31:479–509.

Huttenlocher PR. 1979. Synaptic density in human frontal cortex - developmental changes and effects of aging. Brain Res 163:195f Neu [PubMed: 427544]

Kawa MP, Machalinska A, Roginska D, Machalinski B. 2014. Complement system in pathogenesis of AMD: dual player in degeneration and protection of retinal tissue. J Immunol Res 2014:483960. [PubMed: 25276841]

Klein RJ, Zeiss C, Chew EY, Tsai J-Y, Sackler RS, Haynes C, Henning AK, SanGiovanni JP, Mane SM, Mayne ST, Bracken MB, Ferris FL, Ott J, Barnstable C, Hoh J. 2005. Complement factor H polymorphism in age-related macular degeneration. Science 308:385–389. [PubMed: 15761122]

Lehrman EK, Wilton DK, Litvina EY, Welsh CA, Chang ST, Frouin A, Walker AJ, Heller MD, Umemori H, Chen C, Stevens B. 2018. CD47 Protects Synapses from Excess Microglia-Mediated Pruning during Development. Neuron 100:120–134.e6. [PubMed: 30308165]

Li Q, Barres BA. 2018. Microglia and macrophages in brain homeostasis and disease. Nature Reviews Immunology 18:225. 201

Li T, Chiou B, Gilman CK, Luo R, Koshi T, Yu D, Oak HC, Giera S, Johnson-Venkatesh E, Muthukumar AK, Stevens B, Umemori H, Piao X. 2020. A splicing isoform of GPR56 mediates microglial synaptic refinement via phosphatidylserine binding. EMBO J 39:e104136. [PubMed: 32452062]

Lowery RL, Tremblay M-E, Hopkins BE, Majewska AK. 2017. The microglial fractalkine receptor is not required for activity-dependent plasticity in the mouse visual system. Glia 65:1744–1761. [PubMed: 28836393]

Lui H, Zhang J, Makinson SR, Cahill MK, Kelley KW, Huang H-Y, Shang Y, Oldham MC, Martens LH, Gao F, Coppola G, Sloan SA, Hsieh CL, Kim CC, Bigio EH, Weintraub S, Mesulam M-M, Rademakers R, Mackenzie IR, Seeley WW, Karydas A, Miller BL, Borroni B, Ghidoni R, Farese RV, Paz JT, Barres BA, Huang EJ. 2016. Progranulin Deficiency Promotes Circuit-Specific Synaptic Pruning by Microglia via Complement Activation. Cell 165:921–935. [PubMed: 27114033]

Ma Y, Ramachandran A, Ford N, Parada I, Prince DA. 2013. Remodeling of dendrites and spines in the C1q knockout model of genetic epilepsy. Epilepsia 54:1232–1239. [PubMed: 23621154]

Paolicelli RC, Bolasco G, Pagani F, Maggi L, Scianni M, Panzanelli P, Giustetto M, Ferreira TA, Guiducci E, Dumas L, Ragozzino D, Gross CT. 2011. Synaptic Pruning by Microglia Is Necessary for Normal Brain Development. Science 333:1456, Borr [PubMed: 21778362]

Park J, Choi Y, Jung E, Lee S-H, Sohn J-W, Chung W-S. 2021. Microglial MERTK eliminates phosphatidylserine-displaying inhibitory post-synapses. EMBO J:e107121. [PubMed: 34013588]

Penzes P, Cahill ME, Jones KA, VanLeeuwen J-E, Woolfrey KM. 2011. Dendritic spine pathology in neuropsychiatric disorders. Nat Neurosci 14:285–293. [PubMed: 21346746]

Pinto JGA, Jones DG, Murphy KM. 2013. Comparing development of synaptic proteins in rat visual, somatosensory, and frontal cortex. Front Neural Circuits 7:97. [PubMed: 23754984]

Rakic P, Bourgeois JP, Eckenhoff MF, Zecevic N, Goldman-Rakic PS. 1986. Concurrent overproduction of synapses in diverse regions of the primate cerebral cortex. Science 232:232–235. [PubMed: 3952506]

Reinehr S, Gomes SC, Gassel CJ, Asaad MA, Stute G, Schargus M, Dick HB, Joachim SC. 2019. Intravitreal Therapy Against the Complement Factor C5 Prevents Retinal Degeneration in an Experimental Autoimmune Glaucoma Model. Front Pharmacol 10:1381. [PubMed: 31849650]

Riccomagno MM, Kolodkin AL. 2015. Sculpting Neural Circuits by Axon and Dendrite Pruning. Annu Rev Cell Dev Biol 31:779the C [PubMed: 26436703]

Rosen AM, Stevens B. 2010. The role of the classical complement cascade in synapse loss during development and glaucoma. Adv Exp Med Biol 703:75–93. [PubMed: 20711708]

Schafer DP, Lehrman EK, Kautzman AG, Koyama R, Mardinly AR, Yamasaki R, Ransohoff RM, Greenberg ME, Barres BA, Stevens B. 2012. Microglia sculpt postnatal neural circuits in an activity and complement-dependent manner. Neuron 74:691–705. [PubMed: 22632727]

Schartz ND, Tenner AJ. 2020. The good, the bad, and the opportunities of the complement system in neurodegenerative disease. J Neuroinflammation 17:354. [PubMed: 33239010]

Schecter RW, Maher EE, Welsh CA, Stevens B, Erisir A, Bear MF. 2017. Experience-Dependent Synaptic Plasticity in V1 Occurs without Microglial CX3CR1. J Neurosci 37:10541s in an

Sekar A, Bialas AR, de Rivera H, Davis A, Hammond TR, Kamitaki N, Tooley K, Presumey J, Baum M, Van Doren V, Genovese G, Rose SA, Handsaker RE, Schizophrenia Working Group of the Psychiatric Genomics Consortium, Daly MJ, Carroll MC, Stevens B, McCarroll SA. 2016. Schizophrenia risk from complex variation of complement component 4. Nature 530:177–183. [PubMed: 26814963]

Sellgren CM, Sheridan SD, Gracias J, Xuan D, Fu T, Perlis RH. 2017. Patient-specific models of microglia-mediated engulfment of synapses and neural progenitors. Mol Psychiatry 22:170chiat [PubMed: 27956744]

Shen K, Scheiffele P. 2010. Genetics and Cell Biology of Building Specific Synaptic Connectivity. Annual Review of Neuroscience 33:473–507.

Shi Q, Chowdhury S, Ma R, Le KX, Hong S, Caldarone BJ, Stevens B, Lemere CA. 2017. Complement C3 deficiency protects against neurodegeneration in aged plaque-rich APP/PS1 mice. Sci Transl Med 9:eaaf6295. [PubMed: 28566429]

Soteros BM, Cong Q, Palmer CR, Sia G-M. 2018. Sociability and synapse subtype-specific defects in mice lacking SRPX2, a language-associated gene. PLoS ONE 13:e0199399. [PubMed: 29920554]

Stasi K, Nagel D, Yang X, Wang R-F, Ren L, Podos SM, Mittag T, Danias J. 2006. Complement component 1Q (C1Q) upregulation in retina of murine, primate, and human glaucomatous eyes. Invest Ophthalmol Vis Sci 47:1024–1029. [PubMed: 16505037]

Stevens B, Allen NJ, Vazquez LE, Howell GR, Christopherson KS, Nouri N, Micheva KD, Mehalow AK, Huberman AD, Stafford B, Sher A, Litke AM, Lambris JD, Smith SJ, John SW, Barres BA. 2007. The classical complement cascade mediates CNS synapse elimination. Cell 131:1164–78. [PubMed: 18083105]

Stevens B, Allen NJ, Vazquez LE, Howell GR, Cformation. Journal of Cell Biology [Internet] 220. Available from: 10.1083/jcb.202103052

Torborg CL, Feller MB. 2004. Unbiased analysis of bulk axonal segregation patterns. J Neurosci Methods 135:17m: h [PubMed: 15020085]

Torborg CL, Hansen KA, Feller MB. 2005. High frequency, synchronized bursting drives eye-specific segregation of retinogeniculate projections. Nat Neurosci 8:72–78. [PubMed: 15608630]

Tremblay M-È, Lowery RL, Majewska AK. 2010. Microglial Interactions with Synapses Are Modulated by Visual Experience. PLOS Biology 8:e1000527. [PubMed: 21072242]

Vainchtein ID, Chin G, Cho FS, Kelley KW, Miller JG, Chien EC, Liddelow SA, Nguyen PT, Nakao-Inoue H, Dorman LC, Akil O, Joshita S, Barres BA, Paz JT, Molofsky AB, Molofsky AV. 2018. Astrocyte-derived Interleukin-33 promotes microglial synapse engulfment and neural circuit development. Science 359:1269–1273. [PubMed: 29420261]

Vasek MJ, Garber C, Dorsey D, Durrant DM, Bollman B, Soung A, Yu J, Perez-Torres C, Frouin A, Wilton DK, Funk K, DeMasters BK, Jiang X, Bowen JR, Mennerick S, Robinson JK, Garbow JR, Tyler KL, Suthar MS, Schmidt RE, Stevens B, Klein RS. 2016. A complement–microglial axis drives synapse loss during virus-induced memory impairment. Nature 534:538–543. [PubMed: 27337340]

Wang C, Yue H, Hu Z, Shen Y, Ma J, Li J, Wang X-D, Wang L, Sun B, Shi P, Wang L, Gu Y. 2020. Microglia mediate forgetting via complement-dependent synaptic elimination. Science 367:688–694. [PubMed: 32029629]

Welsh CA, Stephany C-Shen Y, Ma J, Li J, Wang X-D, Wang L, Sun B, Shi P, Wang L, Gu Y. 2020. Microglia mediate forgetting via complement-dependent synaptic e

Werneburg S, Jung J, Kunjamma RB, Ha S-K, Luciano NJ, Willis CM, Gao G, Biscola NP, Havton LA, Crocker SJ, Popko B, Reich DS, Schafer DP. 2020. Targeted Complement Inhibition at Synapses Prevents Microglial Synaptic Engulfment and Synapse Loss in Demyelinating Disease. Immunity 52:167–182.e7. [PubMed: 31883839]

Williams PA, Tribble JR, Pepper KW, Cross SD, Morgan BP, Morgan JE, John SWM, Howell GR. 2016. Inhibition of the classical pathway of the complement cascade prevents early dendritic and synaptic degeneration in glaucoma. Mol Neurodegener 11:26. [PubMed: 27048300]

Wilton DK, Dissing-Olesen L, Stevens B. 2019. Neuron-Glia Signaling in Synapse Elimination. Annual Review of Neuroscience 42:107ay of

de Wit J, Ghosh A. 2016. Specification of synaptic connectivity by cell surface interactions. Nat Rev Neurosci 17:4–4. [PubMed: 26656256]

Yilmaz M, Yalcin E, Presumey J, Aw E, Ma M, Whelan CW, Stevens B, McCarroll SA, Carroll MC. 2021. Overexpression of schizophrenia susceptibility factor human complement C4A promotes excessive synaptic loss and behavioral changes in mice. Nat Neurosci 24:214–224. [PubMed: 33353966]

Zhan Y, Paolicelli RC, Sforazzini F, Weinhard L, Bolasco G, Pagani F, Vyssotski AL, Bifone A, Gozzi A, Ragozzino D, Gross CT. 2014. Deficient neuron-microglia signaling results in impaired functional brain connectivity and social behavior. Nat Neurosci 17:400–406. [PubMed: 24487234]

Main Points:

1. C1q and SRPX2 regulate synapse elimination in the visual thalamus but not the visual cortex in early development
2. The regulation of synapse elimination by SRPX2 requires C1q.

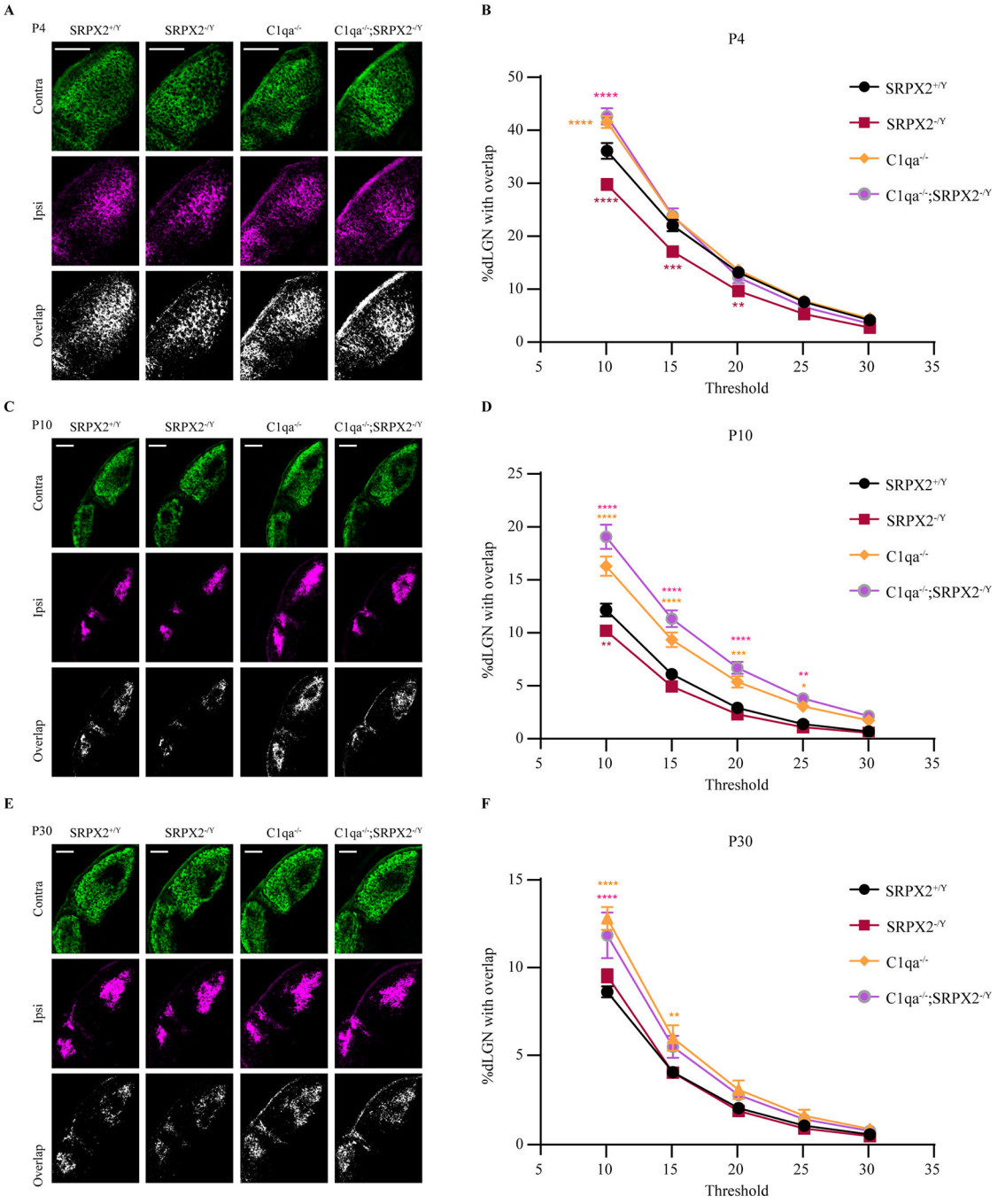

Figure 1: C1q and SRPX2 regulate synapse elimination in the dLGN.

RGC afferents in the dLGN were labelled by injecting CTB-Alexa-488 and CTB-Alexa-555 into the left eye and right eye, respectively (A, C, E), Representative P4 (A), P10 (C), and P30 (E) CTB-labelled dLGN images. Scale bars 200 μm. (B, D, F), Multi-threshold analysis of percentage of P4 (B), P10 (D), and P30 (F) dLGN area receiving inputs from both eyes. Data plotted as mean ± S.E.M., and analyzed by two-way ANOVA and two-tailed Dunnett's post-hoc test with means compared to $SRPX2^{+/Y}$ control. ****$p < 0.0001$, ***$p < 0.001$, **$p < 0.01$, $SRPX2^{+/Y}$, n=6 animals; $SRPX2^{-/Y}$, n=8 animals; $C1qa^{-/-}$,

n=8 animals; C1qa$^{-/-}$;SRPX2$^{-/Y}$, n=4 animals (B). ****p < 0.0001, ***p < 0.001, **p < 0.01, *p < 0.05, SRPX2$^{+/Y}$, n=7 animals; SRPX2$^{-/Y}$, n=7 animals; C1qa$^{-/-}$, n=8 animals; C1qa$^{-/-}$;SRPX2$^{-/Y}$, n=3 animals (D). ****p < 0.0001, **p < 0.01, SRPX2$^{+/Y}$, n=4 animals; SRPX2$^{-/Y}$, n=4 animals; C1qa$^{-/-}$, n=4 animals; C1qa$^{-/-}$;SRPX2$^{-/Y}$, n=3 animals (F).

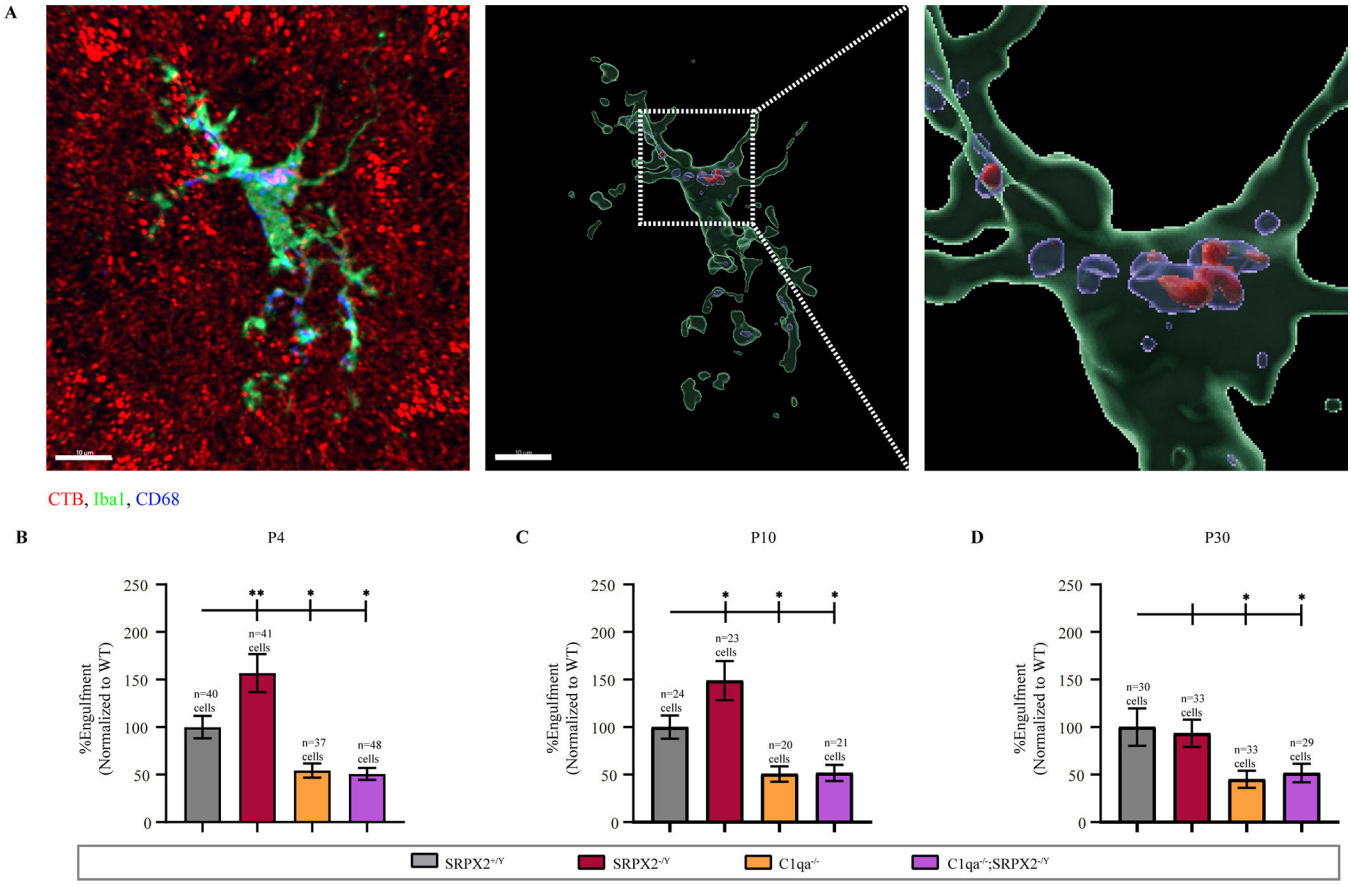

Figure 2: C1q and SRPX2 regulate microglial engulfment of retinogeniculate synapses in the dLGN.

RGC axons were labelled with CTB-Alexa-555, and microglia engulfment of RGC axons were measured.(A) Left panel: representative image of a microglia from the dLGN of a P4 SRPX2$^{+/Y}$ mouse, stained for microglial marker Iba1 (green), lysosome marker CD68 (blue), and CTB-Alexa-555 (red). Scale bar 10 μm. Middle panel: 3D reconstruction of microglia, showing volume of microglia in green, volume of lysosome in blue, and volume of CTB-Alexa-555 in red. Scale bar 10 μm. Right panel: enlargement of cell body of microglia. (B, C, D) Quantitation of percentage of microglial lysosome volume containing CTB-555 at P4 (B), at P10 (C), at P30 (D), plotted as mean ± S.E.M., and analyzed by one-way ANOVA followed by two-tailed Dunnett's post-hoc test with means compared to SRPX2$^{+/Y}$ control. * $p<0.05$, ** $p<0.01$. SRPX2$^{+/Y}$, n=40 cells from 4 mice; SRPX2$^{-/Y}$, n=41 cells from 4 mice; C1qa$^{-/-}$, n=37 cells from 4 mice; C1qa$^{-/-}$;SRPX2$^{-/Y}$, n=48 cells from 4 mice (B); * $p<0.05$. SRPX2$^{+/Y}$, n=24 cells from 4 mice; SRPX2$^{-/Y}$, n=23 cells from 4 mice; C1qa$^{-/-}$, n=20 cells from 4 mice; C1qa$^{-/-}$;SRPX2$^{-/Y}$, n=21 cells from 4 mice (C); * $p<0.05$. SRPX2$^{+/Y}$, n=30 cells from 3 mice; SRPX2$^{-/Y}$, n=33 cells from 3 mice; C1qa$^{-/-}$, n=33 cells from 3 mice; C1qa$^{-/-}$;SRPX2$^{-/Y}$, n=29 cells from 3 mice (D).

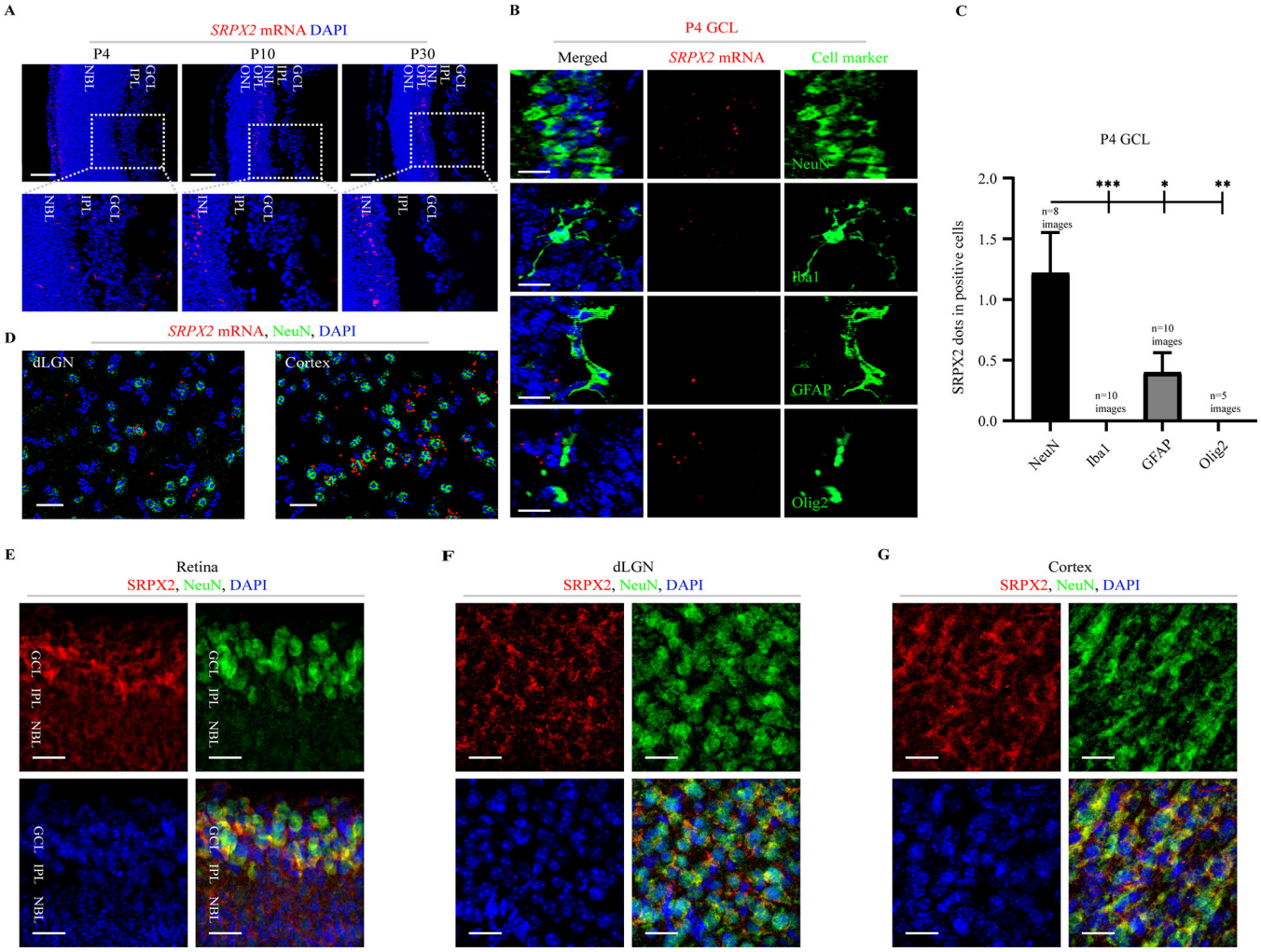

Figure 3: Expression of SRPX2 in the developing mouse retina, dLGN, and visual cortex

RNAscope ISH of SRPX2 in the retino-geniculo-cortical visual pathway. (A) Representative images of RNAscope ISH for SRPX2 mRNA (red) in the mouse retina at P4, P10, and P30. Nuclei were stained with DAPI (blue). Scale bar 100 μm. (B) Representative images of combined RNAscope ISH for SRPX2 mRNA (red) and immunostaining for cell-specific markers (green) for neurons (NeuN), microglia (Iba1), astrocytes (GFAP), and oligodendrocytes (Olig2) in the mouse retina ganglion cell layer at P4. Nuclei were stained with DAPI (blue). Scale bar 10 μm. (C) Quantification of ISH for SRPX2 mRNA in the mouse retina ganglion cell layer at P4. The number of SRPX2 mRNA puncta colocalized with the DAPI area of each cell type is plotted as the mean ± S.E.M. Data were analyzed using one-way ANOVA with two-sided Dunnett's post hoc test comparing all means to NeuN. NeuN, n = 8 images from 3 mice, Iba1, n = 10 images from 3 mice, GFAP, n = 10 images from 3 mice, Olig2, n = 5 images from 3 mice, *$p < 0.05$, **$p < 0.01$, ***$p < 0.001$. (D) RNAscope ISH for SRPX2 mRNA (red) combined with immunostaining for neuron marker NeuN (green) and DAPI (blue) in the dLGN and layer 4 of the primary visual cortex. Scale bar 25 μm. (E) Representative images of SRPX2 (red) and neurons (NeuN, green) in the mouse retina at P4. Nuclei were stained with DAPI (blue). Scale bar 20 μm. (F)

Representative images of SRPX2 (red) and neurons (NeuN, green) in the mouse dLGN at P4. Nuclei were stained with DAPI (blue). Scale bar 20 μm. (G) Representative images of SRPX2 (red) and neurons (NeuN, green) in the mouse visual cortex at P4. Nuclei were stained with DAPI (blue). Scale bar 20 μm.

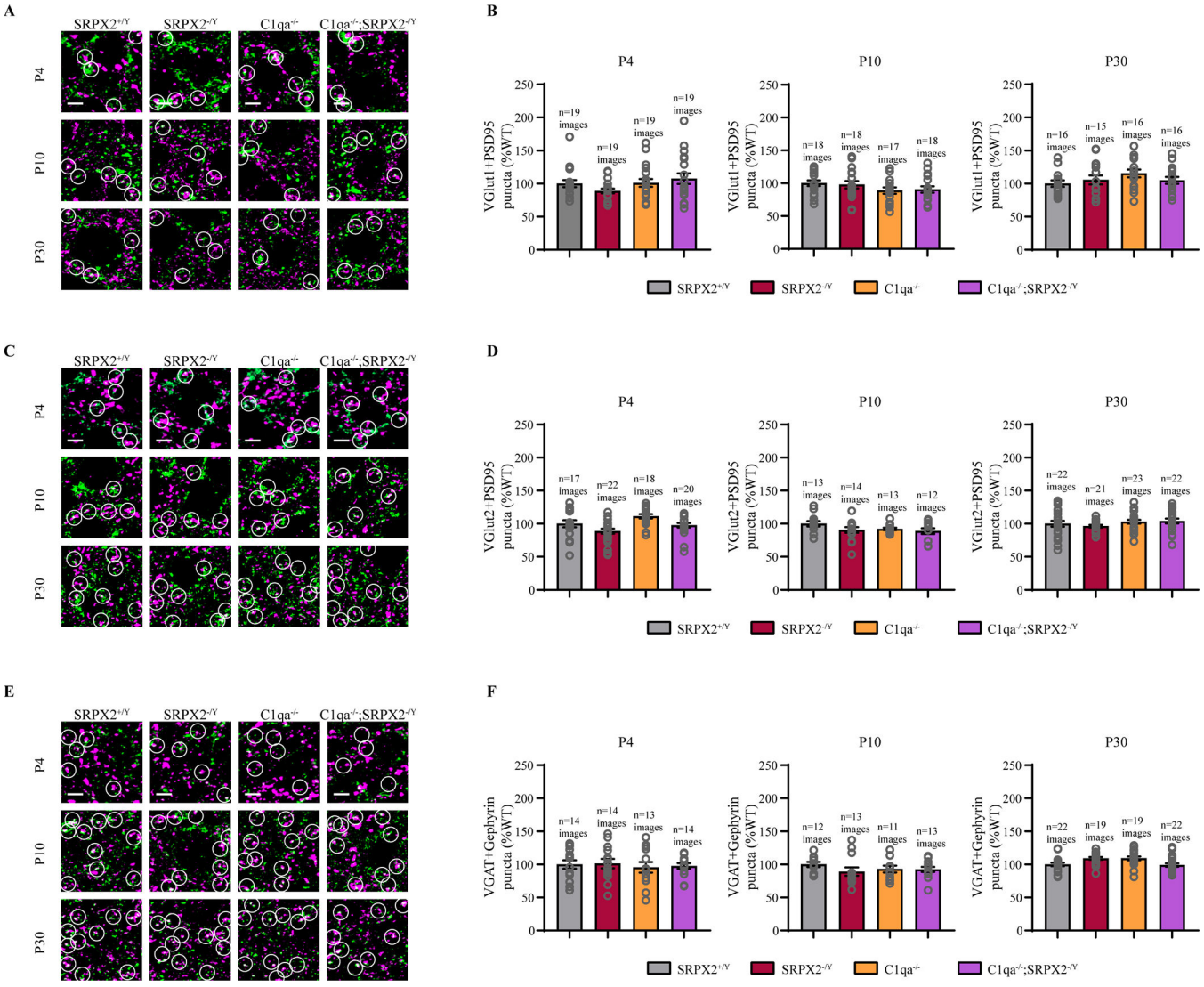

Figure 4: C1q and SRPX2 do not regulate synapse elimination in layer 4 of the primary visual cortex during early development.

Layer 4 visual cortex of brain slices from SRPX2$^{+/Y}$, SRPX2$^{-/Y}$, C1qa$^{-/-}$, C1qa$^{-/-}$;SRPX2$^{-/Y}$ mice were stained for various synaptic markers at P4, P10, and P30. (A, C, E) Representative images of layer 4 visual cortex immunostained for excitatory presynaptic marker VGlut1 (magenta) and excitatory postsynaptic marker PSD95 (green) (A), excitatory presynaptic marker VGlut2 (magenta) and excitatory postsynaptic marker PSD95 (green) (C), and inhibitory presynaptic marker VGAT (magenta) and inhibitory postsynaptic marker gephyrin (green) (E). Circles indicate colocalized presynaptic and postsynaptic puncta. Scale bar 10 μm. (B, D, F) Quantification of colocalized pre-and-postsynaptic markers VGlut1+PSD95 (B), VGlut2+PSD95 (D), and VGAT+gephyrin (F) at P4, P10 and P30. Data shown as mean ± S.E.M., and analyzed by one-way ANOVA, followed by two-tailed Dunnett's post-hoc test compared to SRPX2$^{+/Y}$ control. For VGlut1+PSD95 (B): at P4, SRPX2$^{+/Y}$, n=19 images from 4 mice; SRPX2$^{-/Y}$, n=19 images from 4 mice; C1qa$^{-/-}$, n=19 images from 4 mice; C1qa$^{-/-}$;SRPX2$^{-/Y}$, n=19 images from 4

mice; at P10, SRPX2$^{+/Y}$, n=18 images from 4 mice; SRPX2$^{-/Y}$, n=18 images from 4 mice; C1qa$^{-/-}$, n=17 images from 4 mice; C1qa$^{-/-}$;SRPX2$^{-/Y}$, n=18 images from 4 mice; at P30, SRPX2$^{+/Y}$, n=16 images from 4 mice; SRPX2$^{-/Y}$, n=15 images from 4 mice; C1qa$^{-/-}$, n=16 images from 4 mice; C1qa$^{-/-}$;SRPX2$^{-/Y}$, n=16 images from 4 mice; For VGlut2+PSD95 (D): at P4, SRPX2$^{+/Y}$, n=17 images from 4 mice; SRPX2$^{-/Y}$, n=22 images from 4 mice; C1qa$^{-/-}$, n=18 images from 4 mice; C1qa$^{-/-}$;SRPX2$^{-/Y}$, n=20 images from 4 mice; at P10, SRPX2$^{+/Y}$, n=13 images from 4 mice; SRPX2$^{-/Y}$, n=14 images from 4 mice; C1qa$^{-/-}$, n=13 images from 4 mice; C1qa$^{-/-}$;SRPX2$^{-/Y}$, n=12 images from 4 mice; at P30, SRPX2$^{+/Y}$, n=22 images from 4 mice; SRPX2$^{-/Y}$, n=21 images from 4 mice; C1qa$^{-/-}$, n=23 images from 4 mice; C1qa$^{-/-}$;SRPX2$^{-/Y}$, n=22 images from 4 mice; For VGAT+Gephyrin (F): at P4, SRPX2$^{+/Y}$, n=14 images from 4 mice; SRPX2$^{-/Y}$, n=14 images from 4 mice; C1qa$^{-/-}$, n=13 images from 4 mice; C1qa$^{-/-}$;SRPX2$^{-/Y}$, n=14 images from 4 mice; at P10, SRPX2$^{+/Y}$, n=12 images from 4 mice; SRPX2$^{-/Y}$, n=13 images from 4 mice; C1qa$^{-/-}$, n=11 images from 4 mice; C1qa$^{-/-}$;SRPX2$^{-/Y}$, n=13 images from 4 mice; at P30, SRPX2$^{+/Y}$, n=22 images from 4 mice; SRPX2$^{-/Y}$, n=19 images from 4 mice; C1qa$^{-/-}$, n=19 images from 4 mice; C1qa$^{-/-}$;SRPX2$^{-/Y}$, n=22 images from 4 mice.

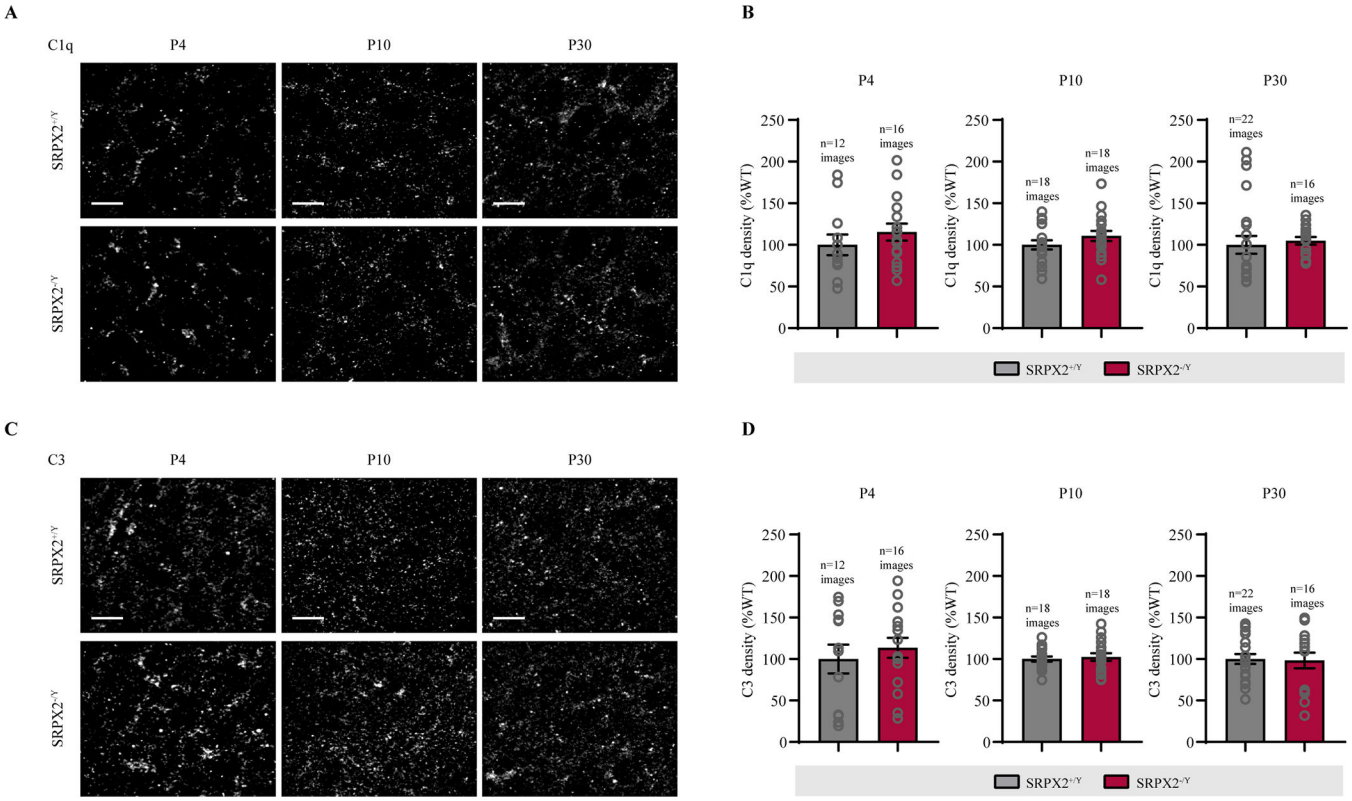

Figure 5: SRPX2 does not regulate complement activation in layer 4 of primary visual cortex during early development.

Layer 4 visual cortex from SRPX2$^{+/Y}$, and SRPX2$^{-/Y}$ mice were stained for C1q and C3 at P4, P10, and P30. (A, C) Representative images of brain slices immunostained for C1q (A) and C3 (C). Scale bar 10 μm. (B, D) Quantification of C1q density (B), and C3 density (D) at P4, P10 and P30. Data shown as mean ± S.E.M., and analyzed by two-tailed unpaired t-test compared to SRPX2$^{+/Y}$ control. For C1q (B) and C3 (D): at P4, SRPX2$^{+/Y}$, n=12 images from 4 mice; SRPX2$^{-/Y}$, n=16 images from 4 mice; at P10, SRPX2$^{+/Y}$, n=18 images from 4 mice; SRPX2$^{-/Y}$, n=18 images from 4 mice; at P30, SRPX2$^{+/Y}$, n=22 images from 4 mice; SRPX2$^{-/Y}$, n=16 images from 4 mice.

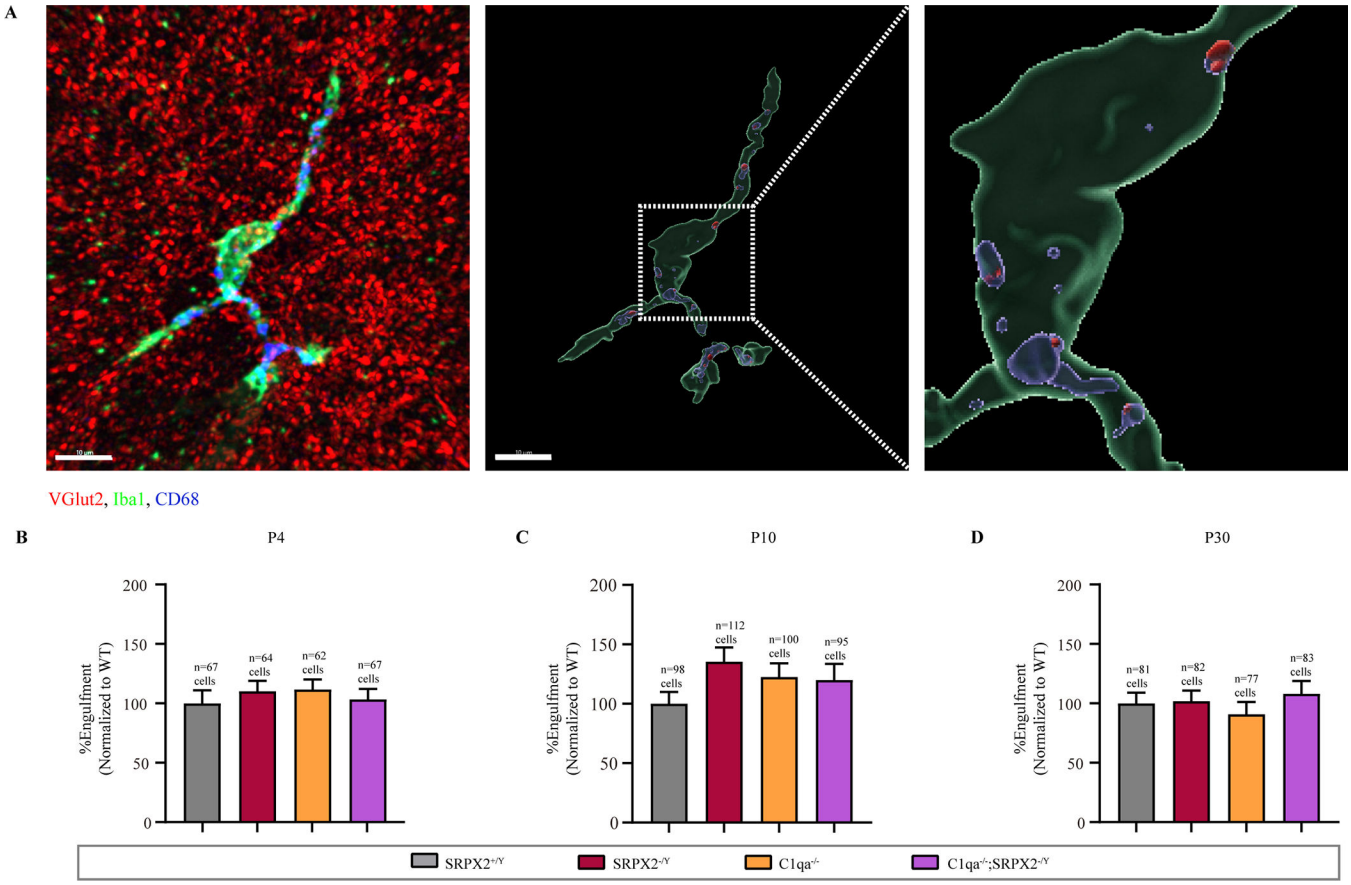

Figure 6: C1q and SRPX2 do not regulate microglia engulfment of synapses in layer 4 of the primary visual cortex during early development.

Brain slices from SRPX2$^{+/Y}$, SRPX2$^{-/Y}$, C1qa$^{-/-}$, C1qa$^{-/-}$;SRPX2$^{-/Y}$ mice were stained for synapse and microglial markers to assess microglial synapse engulfment in layer 4 of the primary visual cortex at P4, P10, and P30. (A) Left panel: representative image of a microglia from the layer 4 of the primary visual cortex of a P4 SRPX2$^{+/Y}$ mouse, stained for microglial marker Iba1 (green), lysosome marker CD68 (blue), and thalamocortical synapse marker VGlut2 (red) from both eyes. Middle panel: 3D reconstruction of microglia, showing volume of microglia in green, volume of lysosome in blue, and volume of VGlut2 in red. Scale bar 10 μm. Right panel: enlargement of cell body of microglia. (B, C, D) Quantitation of percentage of microglial volume containing VGlut2 at P4 (B), at P10 (C), at P30 (D), plotted as mean ± S.E.M., and analyzed by one-way ANOVA followed by two-tailed Dunnett's post-hoc test with means compared to SRPX2$^{+/Y}$ control. SRPX2$^{+/Y}$, n=67 cells from 4 mice; SRPX2$^{-/Y}$, n=64 cells from 4 mice; C1qa$^{-/-}$, n=62 cells from 4 mice; C1qa$^{-/-}$;SRPX2$^{-/Y}$, n=67 cells from 4 mice (B); SRPX2$^{+/Y}$, n=98 cells from 4 mice; SRPX2$^{-/Y}$, n=112 cells from 4 mice; C1qa$^{-/-}$, n=100 cells from 4 mice; C1qa$^{-/-}$;SRPX2$^{-/Y}$, n=95 cells from 4 mice (C); SRPX2$^{+/Y}$, n=81 cells from 3 mice; SRPX2$^{-/Y}$, n=82 cells from 3 mice; C1qa$^{-/-}$, n=77 cells from 3 mice; C1qa$^{-/-}$;SRPX2$^{-/Y}$, n=83 cells from 3 mice (D).